have reported that hippocampal CA3 pyramidal neurons in SERs show a long-lasting depolarizing shift accompanied by repetitive firing with a single stimulation of the mossy fibers [12], and this abnormal excitability is attributable to abnormalities of the L-type Ca^{2+} channels [46]. Morphological studies have demonstrated a decrease in the number of CA3 neurons with maturation, sprouting of mossy fiber in the dentate, and BDNF hyperexpression along the mossy fiber (MF) in a manner analogous to hippocampal sclerosis in complex partial seizures [10].

Here we examined if prophylactic administration of LEV in preseizure-manifesting SERs would protect the hippocampal sclerosis-like change occurred in mature SERs that exhibit tonic convulsion and absence seizures.

2. Materials and methods

2.1. Experimental animals

A total 36 SERs of both sexes at 4 wk of age (prior to manifestation of epileptic seizures) were implanted with an osmotic mini-pump (Alzet, Cupertino, USA) each under the skin at the back for LEV administration. The osmotic mini-pump administered LEV (previously dissolved in physiological saline) or saline alone (controls) for 4 wk at 2.5 μl/h. In Groups A and B, LEV at 420 mg/ml or saline was administered for 4 wk, respectively. To maintain a consistent therapeutic concentration in the animals (10–100 μM), a specific administration regimen was employed [15]: LEV was given at 420 mg/ml for the first 2 wk followed by 840 mg/ml for the subsequent 2 wk, taking into consideration of SER growth in Group B. All animals were kept in individual cages in a room maintained at 23 ± 2 °C and 55 ± 5% relative humidity, and were provided with standard rat chow (MF, Oriental Yeast, Tokyo) and tap water ad libitum. We measured serum LEV concentration at 6- and 8-wk of age. Under ether anesthesia, we took 0.3 ml-blood sample from SER. Serum sample obtained from blood centrifugation (1500 × g, 15 min) was frozen to −20 °C and sent Mitsubishi Chemical Medience Corporation (Tokyo) to measure LEV concentration. Serum LEV was analyzed by gas chromatography/mass spectrometry methods. At 10–11 and 14–15 wk of age, SERs were euthanized with 60 mg/kg sodium pentobarbital. Monitoring regimen was scheduled as described in Fig. 1. Brains of sacrificed animals were isolated and sectioned with the right hemispheres for cell count and BDNF staining, while the left hemispheres were subjected to Timm's staining in the middle after removal and washing in ice-cold saline. All treatment until brain fixation was operated in Hiroshima University. Histological examination using fixed brain was performed in Hiroshima University and Kagoshima University.

2.2. Cell count

After fixation (in 4% paraformaldehyde in 0.1 M phosphate buffer (PB) at pH 7.4) at 4 °C, brains were embedded in paraffin and 4-μm-thick coronal sections were sliced from the anterior to the posterior level. The anteroposterior sections were appropriated according to stereotaxic coordinates of the rat [33]. After hematoxylin-eosin staining, quantification of cell density of coronal sections was performed with a 10 × 10 box with 1 cm^2 microscopic grid. The grid for counting was placed on a well-defined area of the cerebral structure of interest, and counting was carried out with a microscopic enlargement of 200- and 400-fold specifically defined for the respective structures.

Cell counting was performed twice on serial three adjacent sections for each investigated region by a single unbiased observer. Cell counts obtained in every counted field of the 3 sections were pooled and the mean was derived. This procedure was used to minimize potential errors resulting from double-counting. Neurons touching the inferior and edges of the grid were not counted. Counts involved only neurons with cell body larger than 10 μm diameter. Cells with small cell body were considered as glial cells and were not counted.

2.3. Timm's staining

After treatment in 0.1 mol/l PB containing 0.16% Na_2S (pH 7.3) for 1 h, brains were fixed in 0.1 mol/l PB containing 3% glutaraldehyde and 0.16% Na_2S for 1 day before further fixation in 15% sucrose solution for 2 days. The brains were frozen, and cut into 20 μm sagittal sections with a microtome. The sections were mounted on slides and developed in a solution containing 75 ml of 20% gum arabic, 15 ml of a 2% hydroquinone and 3% citric acid mixture, and 1.5 ml of 10% silver nitrate, in the dark for about 1 h. The reaction was terminated by immersing the brain slices in 5% sodium thiosulphate.

2.4. Immunohistochemistry

Tissue sections (thickness: 4 μm) were deparaffinized with xylene, and antigen was harvested with the heat-induced epitope retrieval method using citrate buffer solution (pH 6.0). Degrading effects of endogenous peroxidase were inhibited by dipping the slides into a solution containing a mixture of 30% H_2O_2 (10 ml) and 99% methanol (90 ml) for 30 min. The treated slides were then rinsed and serially washed with 0.01 M phosphate buffered saline (PBS, pH 7.4); 3–5 min were allocated for each washing. An indirect method for immunostaining the antibody, or the labeled streptavidin biotin (SAB) method using Histofine simple stain (Nichirei Company. Tokyo, Japan), was performed with rabbit polyclonal anti-BDNF antibodies (1:100, Dako-Cytomation). Primary antibody incubation was performed overnight at 4 °C, followed by 30-min incubation with secondary antibodies (biotinylated secondary antibodies, SAB kit; Nichirei Company). The reaction mixture was further incubated for 5–10 min with 0.02% diaminobenzidine (DAB tablet; Wako Pure Chemical Industry, Osaka, Japan) and 0.05% H_2O_2 in PBS. All slides were each mounted with a coverslip for storage. Immunohistochemical control sections from two animals underwent similar above-mentioned procedures for all antibodies except for exposure to the primary antibodies.

2.5. Densitometric analysis of immunoreactivity

Images captured by a 3-CCD color video camera (DP 70; Olympus, Tokyo, Japan) mounted on a light microscope (BH 2; Olympus) were relayed to a video monitor and a computer equipped with imaging software (DPC controller, Olympus). The areas of interest selected from the sections and the optical density (OD) of each region (demarcated according to the rat brain atlas) were measured blind by a reader. Images of all areas of interest were captured at 40× or 100× magnification. The color images were transformed to black and white images and analyzed accordingly (ImageJ software; NIH, USA). Immunoreactivity was expressed as OD. Standard transfer curves of the gray level produced by filters of known OD (Kodak, New York, USA) were used for calibration. The mean value of serial 3 sections in each area was calculated. Each value was derived from the difference between the value of region-of-interest and that of white matter of parietal cortex. Each value was corrected to the fourth decimal place.

2.6. Statistical analysis

The values obtained in levetiram-treated SERs were compared with those of saline-treated SER. Group comparisons were determined initially by analysis of variance (ANOVA) for independent groups followed by the Fischer's test.

3. Results

3.1. Serum LEV concentration

Serum LEV concentrations, which were monitored at ages of 6- and 8-wk before operation using the immunofluorescence method, registered 29.1 ± 3.6 and 34.4 ± 3.3 μg/ml in 6- (groups A and B) and 8- (group B) wk-old SERs, respectively. In group A, the LEV concentrations decreased to 18.3 ± 1.1 μg/ml at 8-wk-old. All SERs indicated therapeutic concentrations (10–100 μM) [15] of LEV throughout the prophylactic administration period.

3.2. Hippocampal neurons

The number of CA3 neurons in 14- to 15-wk-old SERs of physiological saline (PS)-treated group B control was significantly ($p < 0.01$) lower (20.7 ± 2.1) than those in 10- to 11-wk-old SERs of groups A control (24.5 ± 2.5) and B control (24.7 ± 1.4). The neuronal counts were comparable to our previous results [10], where surgical intervention did not affect the hippocampal neurons. LEV significantly ($p < 0.01$) inhibited the decreases of CA3 neurons in 10- to 11-wk-old SERs of both groups A (29.5 ± 1.2) and B (30.5 ± 2.5). However, the inhibitory effect was not significantly observed in 14- to 15-wk-old SERs (21.3 ± 2.5), when it was 6 wk after termination of LEV administration (Fig. 2, Table 1).

3.3. Sprouting of mossy fiber in the dentate gyrus

The extent of sprouting was ranked according to the sprouting scores [3]. Sprouting of MF was observed in the inner molecular layer of the dentate gyrus in all PS-treated SERs. Operative effects did not affect MF-sprouting in 14- to 15-wk-old SERs, a finding which is compared with our previous report [10]. In PS treated group, the sprouting scores were higher in SER of group B control

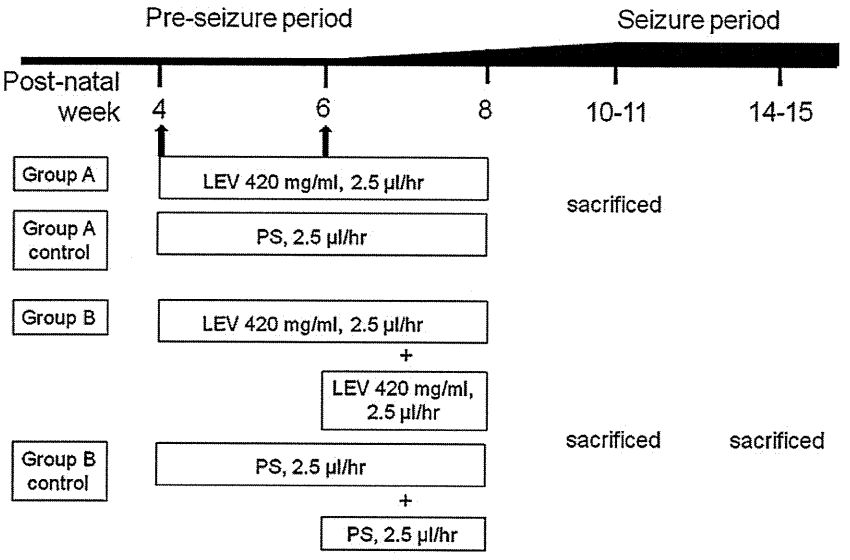

Fig. 1. Regimen for placebo and levetiracetam (LEV) administration: an osmotic mini-pump was embedded in the dorsal skin of each animal, and placebo (physiological saline: PS) or LEV was subcutaneously delivered at a rate of 2.5 μl/h. To maintain a consistent therapeutic concentration in the animals (10–100 μM), the dosage was doubled in the later 2 of the 4-weeks regimen. Refer to details in Section 2.1.

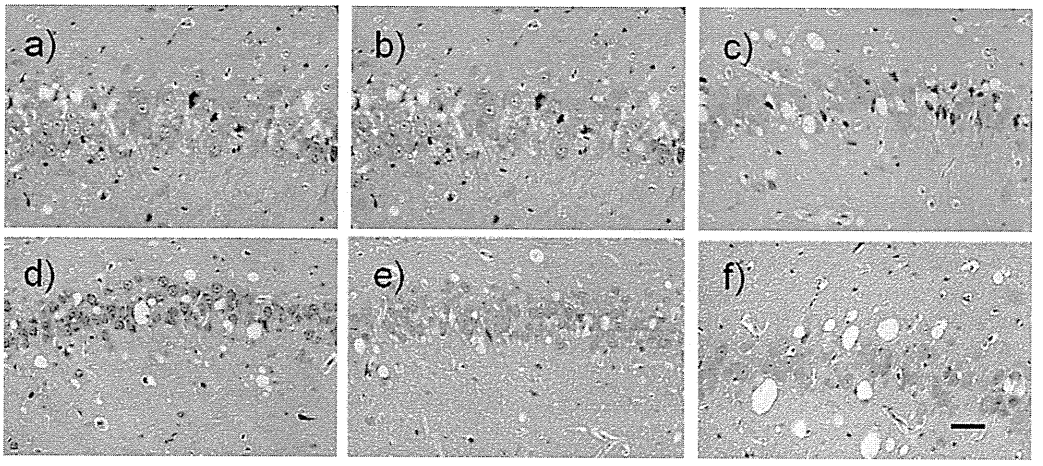

Fig. 2. Effects of levetiracetam on CA3 pyramidal neuron in spontaneously epileptic rat: Groups A, B (10- to 11-weeks-old) and B (14 to 15-weeks-old) were treated with each placebo (a, b, c) or levetiracetam (d, e, f). Number of CA3 neurons in each placebo was less at 14- to 15-weeks-old (c) than at 10- to 11-weeks-old (a, b). Levetiracetam inhibited CA3 neuronal loss at 10- to 11-weeks-old (d, e), but not at 14- to 15-weeks-old (f). Scale bar: 50 μm.

(2.8 ± 1.0) at 14–15 wk of age than those found in groups A control (1.4 ± 0.5) and B control (1.6 ± 0.6) at 10–11 wk of age. LEV significantly ($p < 0.01$) reduced MF sprouting in 10- to 11-wk-old SERs of group B (0.5 ± 0.5), compared with group B control; however this was not the case in group A (1.0 ± 0.6) versus group A control (1.4 ± 0.5). In 14- to 15-wk-old SERs, LEV did not reduce MF scores in group B (2.8 ± 1.0) compared to group B control (3.0 ± 0.9) (Fig. 3, Table 1).

Table 1
Numbers of hippocampal CA3 neurons and Sprouting score of mossy fiber in SERs.

Ages (weeks)	Numeber of neurons		Sprouting score of mossy fiber	
	10–11	14–15	10–11	14–15
Group A				
LEV	29.5 ± 1.2#		1.0 ± 0.6	
Control	24.5 ± 2.5		1.4 ± 0.5	
Group B				
LEV	30.5 ± 2.5#	21.3 ± 2.5	0.5 ± 0.5#	2.8 ± 1.0
Control	24.7 ± 1.4	20.7 ± 2.1	1.6 ± 0.6	3.0 ± 0.9

Average ± S.D.
Control: physiological saline-treated SERs in both group A and group B.
LEV: levetiracetam-treated SERs.
# $p < 0.01$ compared to each physiological saline-treated group.

3.4. Immunoreactivity of BDNF

Analysis of BDNF immunoreactivity (expressed as the optical) was performed after correction for background density. The densitometry levels of BDNF immunoreactivity were higher in the stratum radiatum, pyramidal layer, stratum oriens of CA3, and supragranular layer of the dentate gyrus in 14- to 15-wk-old SERs than those in 10- to 11-wk-old SERs of groups A control and B control. In 10- to 11-wk-old SERs, LEV significantly ($p < 0.05$) reduced BDNF expression in the CA3 pyramidal layer, stratum ratiatum and supragranular layer of the dentate gyrus. LEV given at the higher dose in 10- to 11-wk-old SERs also suppressed BDNF expression in the hilus, granular and inner molecular layer of the dentate gyrus (Fig. 4), CA1 and stratum radiatum. In 14- to 15-wk-old SERs, the significantly inhibitory effects of LEV were still observed except for the CA1, albeit insignificant effects were noted in the hilus and CA1

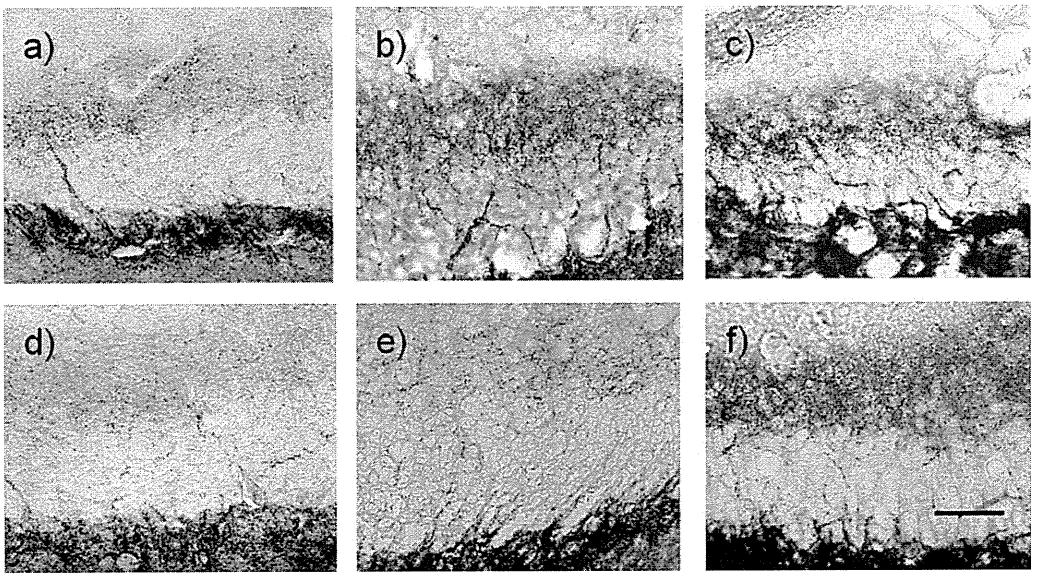

Fig. 3. Effect of levetiracetam on mossy-fiber sprouting in spontaneously epileptic rat: In placebo-treated SER, Timm's staining of the dentate gyrus revealed obvious sprouting in groups A (a) and B (b) at 10- to 11-weeks-old, and B (c) at 14- to 15-weeks-old. Mossy fiber sprouting in each placebo was increased with age (a, b < c). Levetiracetam inhibited mossy-fiber sprouting in both group A and B (d, e) at 10- to 11-weeks-old, but not in group B at 14- to 15-weeks-old (f). Scale bar: 50 μm.

areas (note that, BDNF expression tended to decrease in these areas; Table 2).

4. Discussion

4.1. Profile of levetiracetam

LEV shows a unique, antiepileptic profile: it inhibits seizures in amygdale- and pentylentetrazole-kindled animals [19,26,32] as well as epileptic seizures in genetic epilepsy model animals without affecting acute maximal electroshock or pentylentetrazole-induced seizures. LEV inhibits absence seizures in genetic absence epilepsy rats from Strasbourg (GAERS), groggy rats and spontaneously epileptic rats (SERs) as well as convulsive seizures in audiogenic-seizure sensitive rats [7,14,41].

The antiepileptic mechanisms of action are also completely different from those of the conventional and other newly available antiepileptic drugs: (i) LEV has no effects on voltage-gated ion channels (such as the Na^+, K^+ or Ca^{2+} channels), except for the N-type Ca^{2+} channel [2,4,5,27,48]; and (ii) LEV does not affect the neurotransmitter-related receptors such as glutamate or $GABA_{A/B}$ receptors [20,29]. LEV binds to SV2A protein, which presumably is involved in regulating neurotransmitter release [28]. The antiepileptic action of LEV has been demonstrated to involve SV2A binding, since the inhibitory effect of LEV on seizures induced by 6-Hz electric pulse stimulation is induced in one-half of heterozygous SV2A(+/−) mice and wild-type SV2A(+/+) mice, although SV2A knock-out mice manifest convulsion and die before 2 wk of age [16].

LEV is considered to have some antiepileptogenic effects, since continuous LEV administration during the kindling process inhibits development of both amygdale- and PTZ-kindling as well as kindling in hippocampal kindling Noda epileptic rats (NERs), and genetic epilepsy model animals [13,19,26,32]. Similar results have been reported in the audiogenic kindling model [42]. In addition, our previous study has showed that daily LEV injections in preseizure-manifesting rats (from 4 to 8 wk of age) inhibit the incidence of

Table 2
Expression of BDNF in hippocampus of both physiological saline- and levetiracetam-treated SERs.

	10–11 weeks of age				14–15 weeks of age	
	Control (A)	LEV (A)	Control (B)	LEV (B)	Control (B)	LEV (B)
CA1						
Pyramidal layer	5.5 ± 0.8	5.2 ± 2.6	5.6 ± 0.7	3.5 ± 0.6*	6.3 ± 2.1	6.4 ± 0.7
S. oriens	5.2 ± 2.5	5.2 ± 1.0	5.4 ± 1.0	3.2 ± 0.5*	6.8 ± 1.9	6.5 ± 0.9
CA3						
Pyramidal layer	8.3 ± 1.1	4.6 ± 1.6*	8.1 ± 2.0	2.9 ± 1.3#	9.9 ± 3.9‡	5.2 ± 1.6#
S. oriens	5.1 ± 1.8	4.1 ± 1.4	5.6 ± 1.1	3.4 ± 0.9*	9.0 ± 4.0‡	6.1 ± 1.5*
Hilus	7.2 ± 1.1	6.4 ± 3.7	6.9 ± 1.6	3.0 ± 1.6*	7.3 ± 2.1	3.5 ± 1.9#
S. radiatum	4.4 ± 2.5	2.9 ± 2.2*	4.3 ± 2.5	2.7 ± 1.0*	9.3 ± 3.2‡	4.8 ± 2.9#
Dentate gyrus						
Granular layer	6.8 ± 1.4	4.1 ± 1.0	6.7 ± 1.3	2.7 ± 1.0#	6.8 ± 0.6	4.1 ± 0.9*
IML: sgl	8.3 ± 1.0	5.8 ± 2.0*	8.4 ± 0.1	3.8 ± 0.7#	10.3 ± 1.0‡	5.8 ± 1.0#
IML: outer part	6.0 ± 2.5	4.4 ± 1.2	5.7 ± 2.1	2.5 ± 0.5*	7.7 ± 2.1	5.7 ± 1.2
OML: inner part	4.8 ± 1.3	5.3 ± 0.9	4.8 ± 1.9	3.8 ± 0.8	5.2 ± 1.2	5.4 ± 0.8
OML: outer part	5.2 ± 2.2	5.0 ± 1.4	4.7 ± 1.5	3.5 ± 1.0	5.1 ± 1.3	5.3 ± 0.8

Average ± S.D. ($\times 10^{-3}$).
Control: physiological saline-treated SERs, LEV: levetiracetam-treated SER in both group A and group B, IML: inner molecular layer, OML: outer molecular layer, sgl: suragranular layer.
* $p < 0.05$ compared to each physiological saline-treated group.
# $p < 0.01$ compared to each physiological saline-treated group.
‡ $p < 0.05$ compared to physiological saline-treated SERs at 10- to 11-weeks-old in both group A and group B.

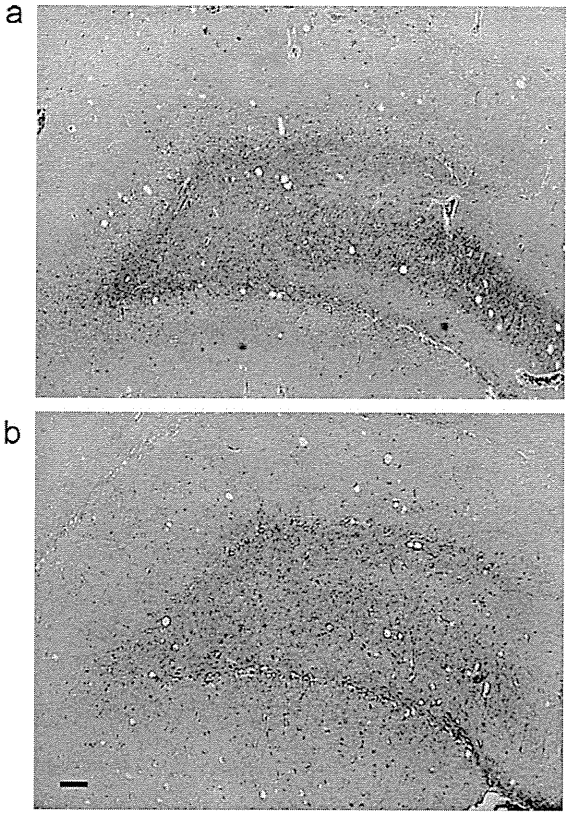

Fig. 4. Effect of levetiracetam on BDNF expression in dentate gyrus of spontaneously epileptic rat: In group B at 10- to 11-weeks-old, levetiracetam-treated SER (b) exhibited less BDNF expression than placebo-treated SER (a) in hilus, granular layer, and inner molecular layer of dentate gyrus. Scale bar: 200 μm.

seizures after 8-wk-old [45]. Epileptogenesis is gradually and progressively formed after establishment of an epileptic focus and progresses with more frequent and repeated seizures [25,38]. Epileptogenesis is gradual after establishment of an epileptic focus and progresses with repeated seizures. During this developmental process, histological changes, such as neuronal loss and neurogenesis, result in reorganization of cell matrixes and axonal/dendritic sprouting [34].

4.2. Neuroprotective effect of levetiracetam in spontaneously epileptic rats

In SERs, which spontaneously exhibit absence-like seizures and convulsive seizures 8–10 wk after birth, a decrease in the number of hippocampal CA3 neurons with age results in repeated seizures [10]. In addition, sprouting reflecting neurogenesis is detected in the inner molecular layer of dentate with age; a phenomenon analogous to neuronal loss. These findings in the genetic epileptic SER coincide well with those in kindling animals [3,35]. Furthermore, in tandem with neuronal loss and sprouting, BDNF expression was enhanced in the hippocampal CA3 pyramidal layer, hilus and granular layer of the dentate gyrus with age. This finding also concurs with that in kindling animal [3,31]. The progressive reorganization of neuronal circuits including neuronal loss, axonal sprouting and gliosis has been reported in human epilepsy [47]. Epileptogenesis in SERs is considered to have been induced at premature ages and by repeated seizures, although SERs are originally devoid of the aspertoacetylase-encoding genes that regulate the metabolism of N-acetyl-L-aspartate (NAA) to form acetate and aspartate [18] and of attractin for myeline formation [23].

Three to 6 wk after termination of 4-wk LEV administration before seizure manifestation, prevention of neuronal loss and inhibition of increased BDNF as well as sprouting were observed in the dentate areas. The increased NAA in SER hippocampus acts on the metabotropic glutamate receptors to induce excessive influxes of Na^+ and Ca^{2+} into CA3 neurons [9,46]. In addition, abnormalities of L-type Ca^{2+} channels in SER hippocampal CA3 neurons, such as lower thresholds for channel-opening and delayed inactivation, induce excessive Ca^{2+} influxes into CA3 neurons [1,46]. The SER CA3 neurons are hypersensitive to glutamate: i.e. glutamate receptor-linked cation channels show a lower opening threshold [8]. All these events are considered to be involved in neuronal death in SER hippocampus, and in turn, induce a compensatory BDNF increase to prevent neuronal death. BDNF is reported to induce hyperexcitable reentrant circuits in the dentate gyrus [22]. It is also likely that the increased BDNF has contributed to induction of sprouting. By inhibiting BDNF increases, LEV may be involved in sprouting inhibition, which at least partly, contributes to hippocampal neuronal reorganization. The neuroprotective effects of LEV have also been observed in kainic acid-induced toxicity in rat [30], and the stroke and head injury model in rat [11,43].

5. Conclusion

Prophylactic treatment with LEV inhibited hippocampal sclerosis-like changes characterized by neuronal loss, sprouting and increased BDNF observed in mature SERs. This inhibitory effect was, at least in part, attributable to LEV suppression of sprouting, an event probably due to up-regulation of BDNF expression and of neuronal death.

Conflict of interest

The authors declare no conflicts of interest.

Acknowledgement

This study was supported by UCB, Inc, Belgium. Levetiracetam was kindly provided by UCB, Inc, Belgium.

References

[1] T. Amano, H. Amano, H. Matsubayashi, K. Ishihara, T. Serikawa, M. Sasa, Enhanced Ca(2+) influx with mossy fiber stimulation in hippocampal CA3 neurons of spontaneously epileptic rats, Brain Res. 910 (2001) 199–203.
[2] J.A. Armijo, M. Shushtarian, E.M. Valdizan, A. Cuadrado, I. de las Cuevas, J. Adín, Ion channels and epilepsy, Curr. Pharm. Des. 11 (2005) 1975–2003.
[3] J.E. Cavazos, I. Das, T.P. Sutula, Neuronal loss induced in limbic pathways by kindling: evidence for induction of hippocampal sclerosis by repeated brief seizures, J. Neurosci. 14 (1994) 3106–3121.
[4] P. Czapinski, B. Blaszczyk, S.J. Czuczwar, Mechanisms of action of antiepileptic drugs, Curr. Top. Med. Chem. 5 (2005) 3–14.
[5] A.C. Errington, T. Stohr, G. Lees, Voltage gated ion channels: target for anticonvulsant drugs, Curr. Top. Med. Chem. 5 (2005) 15–30.
[6] P. Genton, B. Van Vleymen, Piracetam and levetiracetam: close structural similarities but different pharmacological and clinical profiles, Epileptic Disord. 2 (2000) 99–105.
[7] A.J. Gower, E. Hirsch, A. Boehrer, M. Noyer, C. Marescaux, Effects of levetiracetam, a novel antiepileptic drug, on convulsant activity in two genetic rat models of epilepsy, Epilepsy Res. 22 (1995) 207–213.
[8] R. Hanaya, M. Sasa, H. Ujihara, K. Ishihara, T. Serikawa, K. Iida, T. Akimitsu, K. Arita, K. Kurisu, Suppression by topiramate of epileptiform burst discharges in hippocampal CA3 neurons of spontaneously epileptic rat in vitro, Brain Res. 789 (1998) 274–282.
[9] R. Hanaya, Y. Kiura, K. Kurisu, N. Sakai, T. Serikawa, M. Sasa, N-acetyl-L-aspartate activates hippocampal CA3 neurons in rodent slice preparations, Brain Res. Bull. 75 (2008) 663–667.
[10] R. Hanaya, M. Sasa, S. Sugata, M. Tokudome, T. Serikawa, K. Kurisu, K. Arita, Hippocampal cell loss and propagation of abnormal discharges accompanied with the expression of tonic convulsion in the spontaneously epileptic rat, Brain Res. 1328 (2010) 171–180.

[11] E. Hanon, H. Klitgaard, Neuroprotective properties of the novel antiepileptic drug levetiracetam in the rat middle cerebral artery occlusion model of focal cerebral ischemia, Seizure 10 (2001) 287–293.
[12] K. Ishihara, M. Sasa, T. Momiyama, H. Ujihara, J. Nakamura, T. Serikawa, J. Yamada, S. Takaori, Abnormal excitability of hippocampal CA3 pyramidal neurons of spontaneously epileptic rats (SER), a double mutant, Exp. Neurol. 119 (1993) 287–290.
[13] Y. Ishimaru, S. Chiba, T. Serikawa, M. Sasa, H. Inaba, Y. Tamura, T. Ishimoto, H. Takasaki, K. Sakamoto, K. Yamaguchi, Effects of levetiracetam on hippocampal kindling in Noda epileptic rats, Brain Res. 1309 (2010) 104–109.
[14] C. Ji-qun, K. Ishihara, T. Nagayama, T. Serikawa, M. Sasa, Long-lasting antiepileptic effects of levetiracetam against epileptic seizures in the spontaneously epileptic rat (SER): differentiation of levetiracetam from conventional antiepileptic drugs, Epilepsia 46 (2005) 1362–1370.
[15] S.I. Johannessen, D. Battino, D.J. Berry, M. Bialer, G. Kramer, T. Tomson, P.N. Patsalos, Therapeutic drug monitoring of the newer antiepileptic drugs, Ther. Drug Monit. 25 (2003) 347–363.
[16] R.M. Kaminski, M. Gillard, K. Leclercq, E. Hanon, G. Lorent, D. Dassesse, A. Matagne, H. Klitgaard, Proepileptic phenotype of SV2A-deficient mice is associated with reduced anticonvulsant efficacy of levetiracetam, Epilepsia 50 (2009) 1729–1740.
[17] D.G. Kasteleijn-Nolst Trenité, E. Hirsc, Levetiracetam: preliminary efficacy in generalized seizures, Epileptic Disord. Suppl. 1 (2003) 39–44.
[18] K. Kitada, T. Akimitsu, Y. Shigematsu, A. Kondo, T. Maihara, N. Yokoi, T. Kuramoto, M. Sasa, T. Serikawa, Accumulation of N-acetyl-L-aspartate in the brain of the tremor rat, a mutant exhibiting absence-like seizure and spongiform degeneration in the central nervous system, J. Neurochem. 74 (2000) 2512–2519.
[19] H. Klitgaard, A. Matagne, J. Gobert, E. Wülfert, Evidence for a unique profile of levetiracetam in rodent models of seizures and epilepsy, Eur. J. Pharmacol. 353 (1998) 191–206.
[20] H. Klitgaard, Levetiracetam: the preclinical profile of a new class of antiepileptic drugs? Epilepsia 42 (Suppl. 4) (2001) 13–18.
[21] M. Knipper, L.S. Leung, D. Zhao, R.J. Rylett, Short-term modulation of glutamatergic in adult rat hippocampus by NGF, Neuroreport 5 (1994) 2433–2436.
[22] R. Koyama, M.K. Yamada, S. Fujisawa, R. Katoh-Semba, N. Matsuki, Y. Ikegaya, Brain-derived neurotrophic factor induces hyperexcitable reentrant circuits in the dentate gyrus, J. Neurosci. 24 (2004) 7215–7224.
[23] T. Kuramoto, K. Kitada, T. Inui, Y. Sasaki, K. Ito, T. Hase, S. Kawagachi, Y. Ogawa, K. Nakao, G.S. Barsh, M. Nagao, T. Ushijima, T. Serikawa, Attractin/mahogany/zitter plays a critical role in myelination of the central nervous system, Proc. Natl. Acad. Sci. U. S. A. 98 (2001) 559–564.
[24] I. Leppik, M. Morrell, P. Godfroid, C. Arrigo, Seizure-free days observed in randomized placebo-controlled add-on trials with levetiracetam in partial epilepsy, Epilepsia 44 (2003) 1232–1350.
[25] W. Löscher, Animal models of epilepsy for the development of antiepileptogenic and disease-modifying drugs. A comparison of the pharmacology of kindling and post-status epilepticus models of temporal lobe epilepsy, Epilepsy Res. 50 (2002) 105–123.
[26] W. Löscher, D. Hönack, Profile of ucb L059, a novel anticonvulsant drug, in models of partial and generalized epilepsy in mice and rats, Eur. J. Pharmacol. 232 (1993) 147–158.
[27] E.A. Lukyanetz, V.M. Shkryl, P.G. Kostyuk, Selective blockade of N-type calcium channels by levetiracetam, Epilepsia 43 (2002) 9–18.
[28] B.A. Lynch, N. Lambeng, K. Nocka, P. Kensel-Hammes, S.M. Bajjalieh, A. Matagne, B. Fuks, The synaptic vesicle protein SV2A is the binding site for the antiepileptic drug levetiracetam, Proc. Natl. Acad. Sci. U. S. A. 101 (2004) 9861–9866.
[29] D.G. Margineanu, H. Klitgaard, Levetiracetam has no significant gamma-aminobutyric acid-related effect on paired-pulse interaction in the dentate gyrus of rats, Eur. J. Pharmacol. 466 (2003) 255–261.
[30] H. Marini, C. Costa, M. Passaniti, M. Esposito, G.M. Campo, R. Ientile, E.B. Adamo, R. Marini, P. Calabresi, D. Altavilla, L. Minutoli, F. Pisani, F. Squadrito, Levetiracetam protects against kainic acid-induced toxicity, Life Sci. 74 (2004) 1253–1264.
[31] T.R. Mhyre, C.D. Applegate, Persistent regional increases in brain-derived neurotrophic factor in the flurothyl model of epileptogenesis are dependent upon the kindling status of the animal, Neuroscience 121 (2003) 1031–1045.
[32] Y. Ohno, S. Ishihara, R. Terada, T. Serikawa, M. Sasa, Antiepileptogenic and anticonvulsive actions of levetiracetam in a pentylenetetrazole kindling model, Epilepsy Res. 89 (2010) 360–364.
[33] G. Paxinos, C. Watson, The Rat Brain in Stereotaxic Coordinates, 3rd ed., Academic Press, San Diego, 1996.
[34] A. Pitman, T.P. Sutula, Is epilepsy a progressive disorder? Process for new therapeutic approaches in temporal lobe epilepsy, Lancet Neurol. 1 (2002) 173–181.
[35] A. Represa, G. Le Gall La Salle, Y. Ben-Ari, Hippocampal plasticity in the kindling model of epilepsy in rats, Neurosci. Lett. 99 (1989) 345–350.
[36] S. Rhem, P. Mehraein, A.P. Anzil, F. Deerberg, A new rat mutant with detective overhairs and spongy degeneration of the central nervus system: clinical pathological studies, Lab. Animal Sci. 32 (1982) 70–73.
[37] M. Sasa, Y. Ohno, H. Ujihara, Y. Fujita, M. Yoshimura, S. Takaori, T. Serikawa, J. Yamada, Effects of antiepileptic drugs on absence-like and tonic seizures in the spontaneously epileptic rat, a double mutant rat, Epilepsia 29 (1988) 505–513.
[38] M. Sasa, A frontier in epilepsy: novel antiepileptogenetic drugs, J. Pharmacol. Sci. 100 (2006) 487–494.
[39] T. Serikawa, J. Yamada, Epileptic seizures in rats homozygous for two mutations, zitter and tremor, J. Hered. 77 (1986) 441–444.
[40] T. Serikawa, J. Yamada, H. Ujihara, Y. Ohno, M. Sasa, S. Takaori, Ontogeny of absence-like and tonic seizures in the spontaneously epileptic rat, Lab. Anim. 25 (1991) 216–221.
[41] S. Tokuda, N. Sofue, Y. Ohno, M. Sasa, T. Serikawa, Inhibitory effects of levetiracetam on absence seizures in a novel absence-like epilepsy animal model, Groggy rat, Brain Res. 1359 (2010) 298–303.
[42] L.V. Vinogradova, C.M. van Rijn, Anticonvulsive and antiepileptogenic effects of levetiracetam in the audiogenic kindling model, Epilepsia 49 (2008) 1160–1168.
[43] H. Wang, J. Gao, T.F. Lassiter, D.L. McDonagh, H. Sheng, D.S. Warner, J.R. Lynch, D.T. Laskowitz, Levetiracetam is neuroprotective in murine models of closed head injury and subarachnoid hemorrhage, Neurocrit. Care 5 (2006) 71–78.
[44] J. Yamada, T. Serikawa, J. Ishiko, T. Inui, H. Takada, Y. Kawai, A. Okaniwa, Rats with congenital tremor and curled whisker and hair, Exp. Anim. 34 (1985) 183–188.
[45] H.D. Yan, C. Ji-qun, K. Ishihara, T. Nagayama, T. Serikawa, M. Sasa, Separation of antiepileptogenic and antiseizure effects of levetiracetam in the spontaneously epileptic rat (SER), Epilepsia 46 (2005) 1170–1177.
[46] H.D. Yan, K. Ishihara, R. Hanaya, K. Kurisu, T. Serikawa, M. Sasa, Voltage-dependent calcium channel abnormalities in hippocampal CA3 neurons of spontaneously epileptic rats, Epilepsia 48 (2007) 758–764.
[47] D.M. Yilmazer-Hanke, H.K. Wolf, J. Scgeamm, C.E. Elger, O.D. Wiestler, I. Blumcke, Subregional pathology of the amygdale complex and entorhinal region in surgical specimen from patients with pharmacoresistant temporal lobe epilepsy, J. Neuropathol. Exp. Neurol. 59 (2000) 907–920.
[48] C. Zona, I. Niespodziany, C. Marchetti, H. Klitgaard, G. Bernardi, D.G. Margineanu, Levetiracetam does not modulate neuronal voltage-gated Na^+ and T-type Ca^{2+} currents, Seizure 10 (2001) 279–286.

BRAIN RESEARCH 1389 (2011) 161–168

available at www.sciencedirect.com

ScienceDirect

www.elsevier.com/locate/brainres

BRAIN RESEARCH

Research Report

Oligodendroglial pathology in the development of myelin breakdown in the *dmy* mutant rat

Mitsuru Kuwamura[a,*], *Kazuo Inumaki*[a], *Miyuu Tanaka*[a], *Makoto Shirai*[a], *Takeshi Izawa*[a], *Jyoji Yamate*[a], *Robin J.M. Franklin*[b], *Takashi Kuramoto*[c], *Tadao Serikawa*[c]

[a]*Laboratory of Veterinary Pathology, Osaka Prefecture University, Izumisano, Osaka 598–8531, Japan*
[b]*MRC Cambridge Centre for Stem Cell Biology and Regenerative Medicine and Department of Veterinary Medicine, University of Cambridge, Madingley Road, Cambridge CB3 0ES, UK*
[c]*Institute of Laboratory Animals, Graduate School of Medicine, Kyoto University, Sakyo-ku, Kyoto 606–8501, Japan*

ARTICLE INFO

Article history:
Accepted 3 March 2011
Available online 9 March 2011

Keywords:
Dysmyelination
Mutant rat
Oligodendrocyte
Oligodendrocyte progenitor cell
Mitochondria

ABSTRACT

The *dmy* rat is an autosomal recessive mutant that exhibits severe myelin destruction throughout the white matter of the central nervous system. Recently, a point mutation in intron 3 of the Mrs2 has been found in the *dmy* rat. Mrs2 encodes an essential component of the major electrophoretic Mg^{2+} influx system in mitochondria of yeast as well as human cells. In this study, we examined the morphological and numerical changes of oligodendroctyes in the development of myelin destruction in the spinal cord of the *dmy* rat. The number of oligodendrocytes decreases rapidly from 7 weeks of age in the *dmy* rat in accordance with myelin breakdown. Hypertrophic oligodendrocytes were frequently observed, and the cytoplasm was found to be intensely positive for prohibitin and cytochrome oxidase, mitochondrial markers. These data suggest that mitochondrial dysfunction causes a work/compensatory hypertrophy of oligodendrocytes, resulting in direct cell death and leading to myelin destruction.

1. Introduction

Myelin mutant animals, in which myelination is disrupted by a genetic perturbation, have helped with the identification of genes associated with myelination and are useful in increasing our understanding of the function of specific genes in the proper spatial and temporal context of development and disease (Griffiths, 1996). Mutations of structural myelin components have been investigated in many mice and rat models (Al-Saktawi et al., 2003; Griffiths, 1996; Knapp et al., 1986, 2009; Kwiecien et al., 1998). Despite a direct deficit in myelin components, the process of myelination and maintenance of myelin involves complex mechanisms such as the production and transport of myelin-related proteins and lipids. For example, abnormalities of microtubules are considered to be responsible for the hypomyelination and progressive demyelination of the CNS in the *taiep* rat (Duncan et al., 1992; Song et al., 1999). The developmental regulation

* *Corresponding author.* Fax: +81 72 463 5346.
E-mail address: kuwamura@vet.osakafu-u.ac.jp (M. Kuwamura).
Abbreviations: CNS, central nervous system; OPCs, oligodendrocyte progenitor cells; PLP, proteolipid protein

0006-8993/$ – see front matter © 2011 Elsevier B.V. All rights reserved.
doi:10.1016/j.brainres.2011.03.009

and maintenance of myelin have been widely investigated, but many details of these processes remain to be clarified.

The *dmy* rat is an autosomal recessive mutant that exhibits hind limb ataxia and severe myelin destruction throughout the white matter of the central nervous system (CNS) during the late stage of myelination (Kuramoto et al., 1996; Kuwamura et al., 2004). The causative gene of the *dmy* rat is located on rat chromosome 17, homologous to human chromosome 6 and mouse chromosome 13 (Kuramoto et al., 1996). There are no myelin-related or myelin disorder-related genes in the homologous regions of humans and mice, suggesting that the *dmy* rat is a novel myelin mutant and that the causative gene may play a crucial role in the adequate maintenance of myelin. Recently, Kuramoto et al. have revealed that the *dmy* rat has a point mutation generating a novel splicing acceptor site in intron 3 of the Mrs2 gene (Kuramoto et al., 2011). Mrs2 encodes an essential component of the major electrophoretic Mg2+ influx system in mitochondria of yeast as well as human cells, suggesting that the *dmy* mutation is associated with mitochondrial dysfunction.

In this study, we examined the morphological and numerical changes of oligodendroctyes in the development of myelin destruction in the spinal cord of the *dmy* rat. Our results indicate that the number of oligodendrocytes decreases rapidly from 7 weeks of age in the *dmy* rat in accordance with myelin breakdown. Hypertrophic oligodendrocytes were frequently observed, and the cytoplasm was found to be intensely positive for prohibitin and cytochrome oxidase, mitochondrial markers. These data suggest that mitochondrial dysfunction causes a work/compensatory hypertrophy of oligodendrocytes, resulting in direct cell death and leading to myelin destruction.

2. Results

2.1. *Number of oligodendrocytes*

No remarkable histopathological myelin-related lesions were found in the *dmy* rat up to 6 weeks of age. In the *dmy* rat at 7–10 weeks, pale staining areas developed in the white matter of the CNS, with the ventral funiculus being affected particularly severely compared with the dorsal funiculus in the spinal cord (Fig. 1). We investigated the number of oligodendrocytes during the development of myelin destruction in the *dmy* rat by using the proteolipid protein (PLP) in situ hybridization. Until 6 weeks of age, there was no significant difference in the cell number and morphology of PLP-expressing cells between control and *dmy* rats (Fig. 2a–h and Fig. 3a, b). At 7 weeks, the cell density of the oligodendrocytes was significantly decreased and the myelin was rapidly collapsing at 8 weeks in the ventral funiculus (Figs. 2i–p and 3b). The cell density in the dorsal funiculus was retained at all of the weeks examined.

2.2. *Number of OPCs*

The numerical changes of OPCs were examined by NG2 immunohistochemistry (Bu et al., 2004; Kitada and Rowitch, 2006). No morphological abnormalities were found in the NG2-positive cells between control and *dmy* rats until 4 weeks. At 4 weeks, no difference in the cell density of NG2 was observed between control and *dmy* rats in either the dorsal or ventral funiculi. At 6 and 7 weeks, the density of NG2 in the ventral funiculus of *dmy* rat was increased (Fig. 3c, d and Fig. 4a, b); afterwards, at 8 weeks, the density rapidly began to decrease

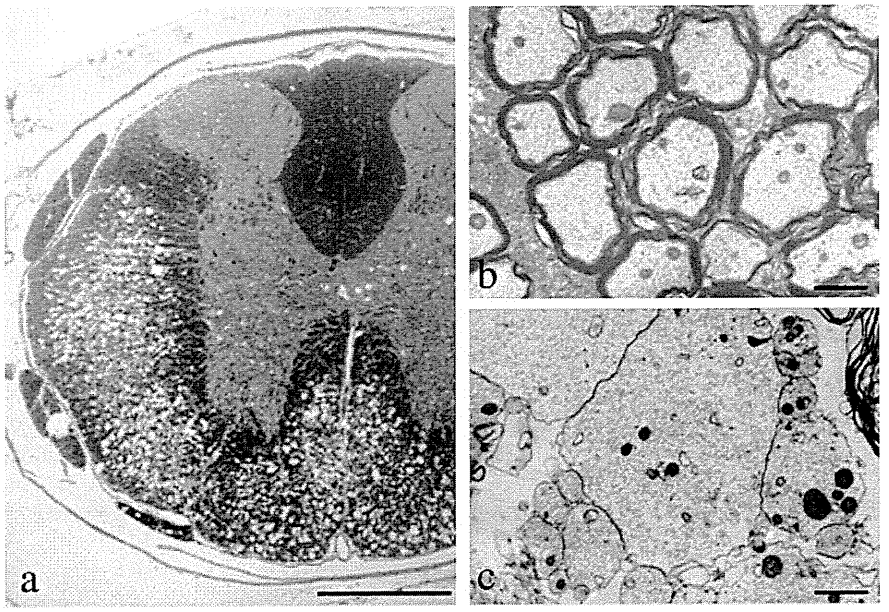

Fig. 1 – Epon embedded toluidine blue stained section of the thoracic spinal cord of 7-week-old *dmy/dmy* rat (a). Marked destruction of myelin is distributed in the lateral and ventral parts, whereas the dorsal funiculus remained normal appearance. Bar, 500 μm. Electron microscopy of the thoracic spinal cord of 7-week-old *dmy/dmy* rat. Normal myelinated axons are found in the dorsal funiculus (b). Many naked axons are seen in the ventral funiculus (c). Bar, 1 μm.

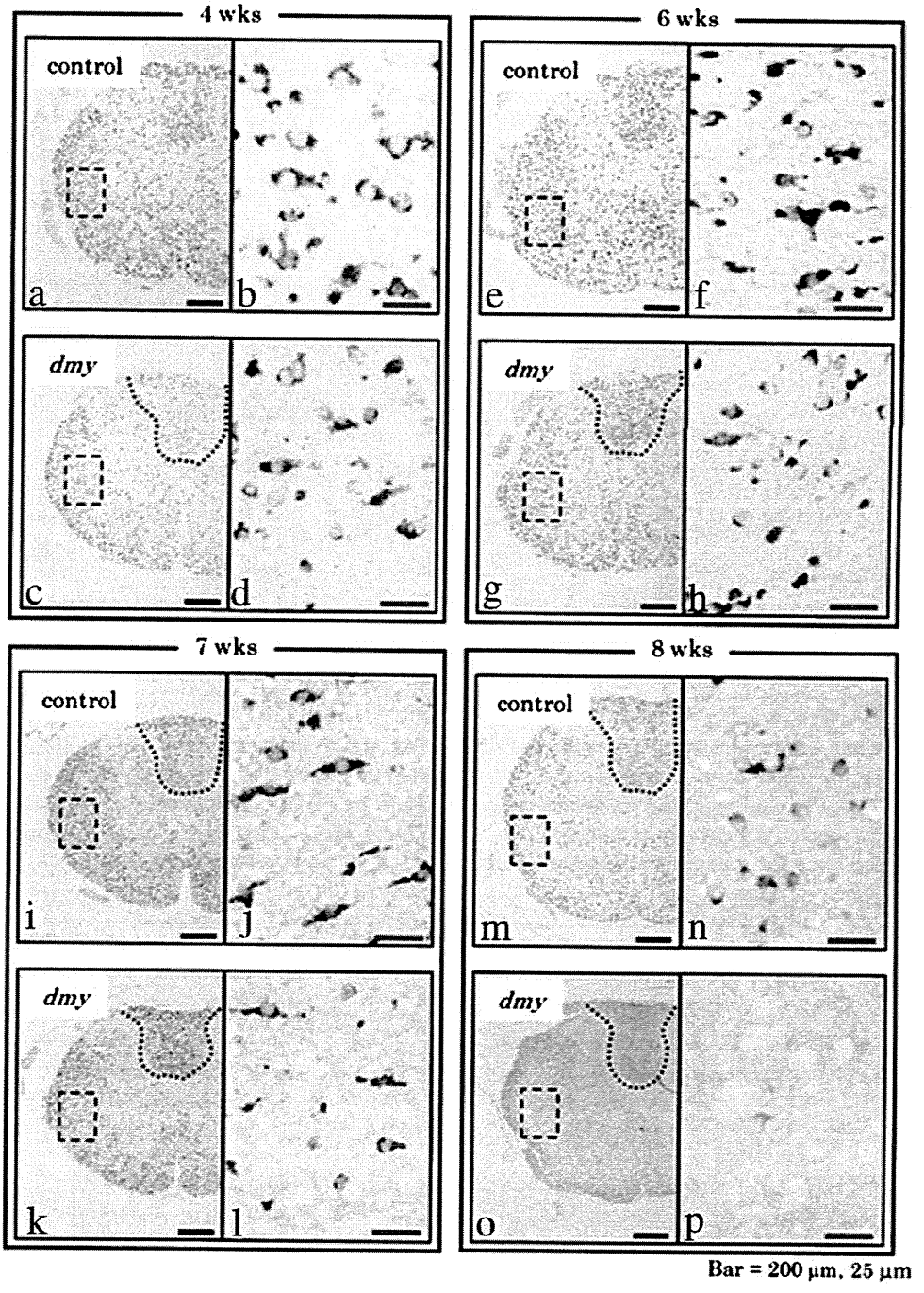

Fig. 2 – In situ hybridization for PLP in the lumbar spinal cord of control (a, b, e, f, i, j, m, n) and *dmy* (c, d, g, h, k, l, o, p) rats. There is no apparent difference between control and *dmy* rats in the morphology of PLP-positive cells until 6 weeks. Marked reduction of PLP-positive cells is found in the lateral funiculus at 8 weeks. The right images are high power views of dot-lined squares of the left images. Black bar, 200 μm; red bar, 25 μm.

(Fig. 3c and d). OLIG2-positive cells were also increased in the ventral funiculus of *dmy* rats (Fig. 4c and d). Immunoreactivity of NG2-positive cells was more conspicuous in the *dmy* rats compared to the control rats at 6 and 7 weeks (Fig. 4a and b). There was no significant difference in the cell density of NG2 in the dorsal funiculus between 6 and 7 weeks.

2.3. *Morphological changes of oligodendrocytes during the development of myelin lesions*

Round to ovoid cells possessing round clear nuclei and abundant light eosinophilic cytoplasm were often found in the white matter of myelin-destructed lesions in the *dmy* rat

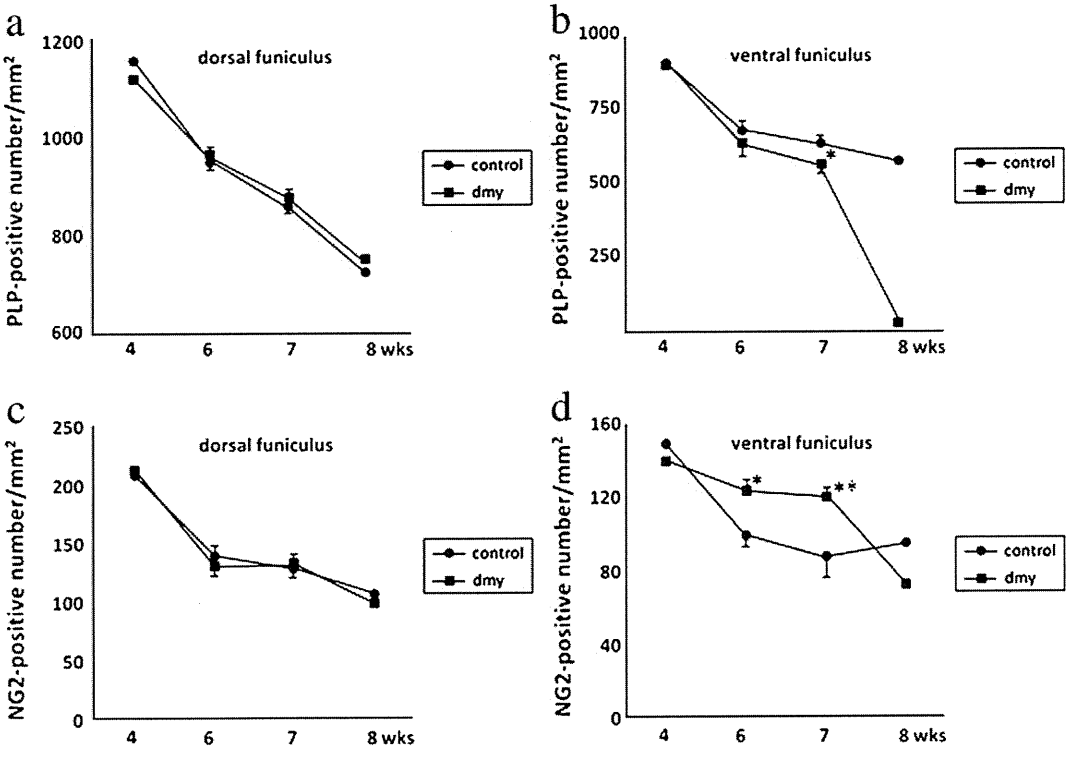

Fig. 3 – The number of PLP-(a, b) and NG2-(c, d) positive cells in the dorsal (a, c) and ventral (b, d) of the spinal cord. There is no difference in cell number between control (circles) and *dmy* (squares) in the dorsal funiculus. At 7 weeks, the cell density of the PLP-positive oligodendrocytes were significantly decreased ($n=3$ in each group) and rapidly decreased at 8 weeks in the ventral funiculus (b). At 6 and 7 weeks, the density of NG2-positive cells in the ventral funiculus of *dmy* rat is significantly increased ($n=3$ in each group) and the density rapidly began to decrease at 8 weeks (d). Presented as the mean ± SD. $^{*}P<0.05$, $^{**}P<0.01$, compared to control rats.

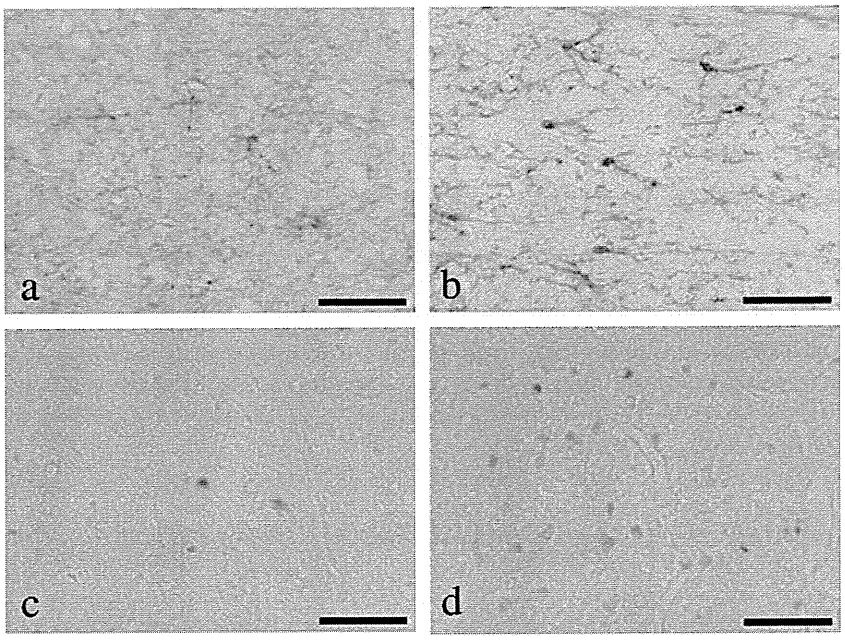

Fig. 4 – NG2 immunohistochemistry in the ventral funiculus of the spinal cord in control (a) and *dmy/dmy* (b) rats aged 7 weeks. Many NG2-positive cells are seen in the *dmy/dmy* rat, compared to the control. NG2-positive cells are intensely stained in *dmy/dmy* rat. Bar, 50 μm. OLIG2 immunohistochemistry in the ventral funiculus of the spinal cord in control (c) and *dmy/dmy* (d) rats aged 7 weeks. Many OLIG2-positive cells are found in the *dmy/dmy* rat compared to the control. Bar, 50 μm.

(Fig. 5a and b). Prohibitin immunohistochemistry revealed that a few positively stained cells were sparsely observed in the white matter of *dmy* rats until 6 weeks and control rats (Fig. 5c), whereas many prohibitin-positive hypertrophic cells were found in the ventral funiculus of *dmy* rats at 7 and 8 weeks (Fig. 5d). These hypertrophic cells were also intensely stained by cytochrome oxidase histochemistry, compared with age-matched control rats (Fig. 5e and f). To identify the origin of hypertrophic cells, serial paraffin sections were stained with prohibitin immunohistochemistry and PLP in situ hybridization. Prohibitin positive hypertrophic cells were expressed PLP mRNA (Fig. 5g and h), indicating that hypertrophic cells are derived from oligodendrocytes.

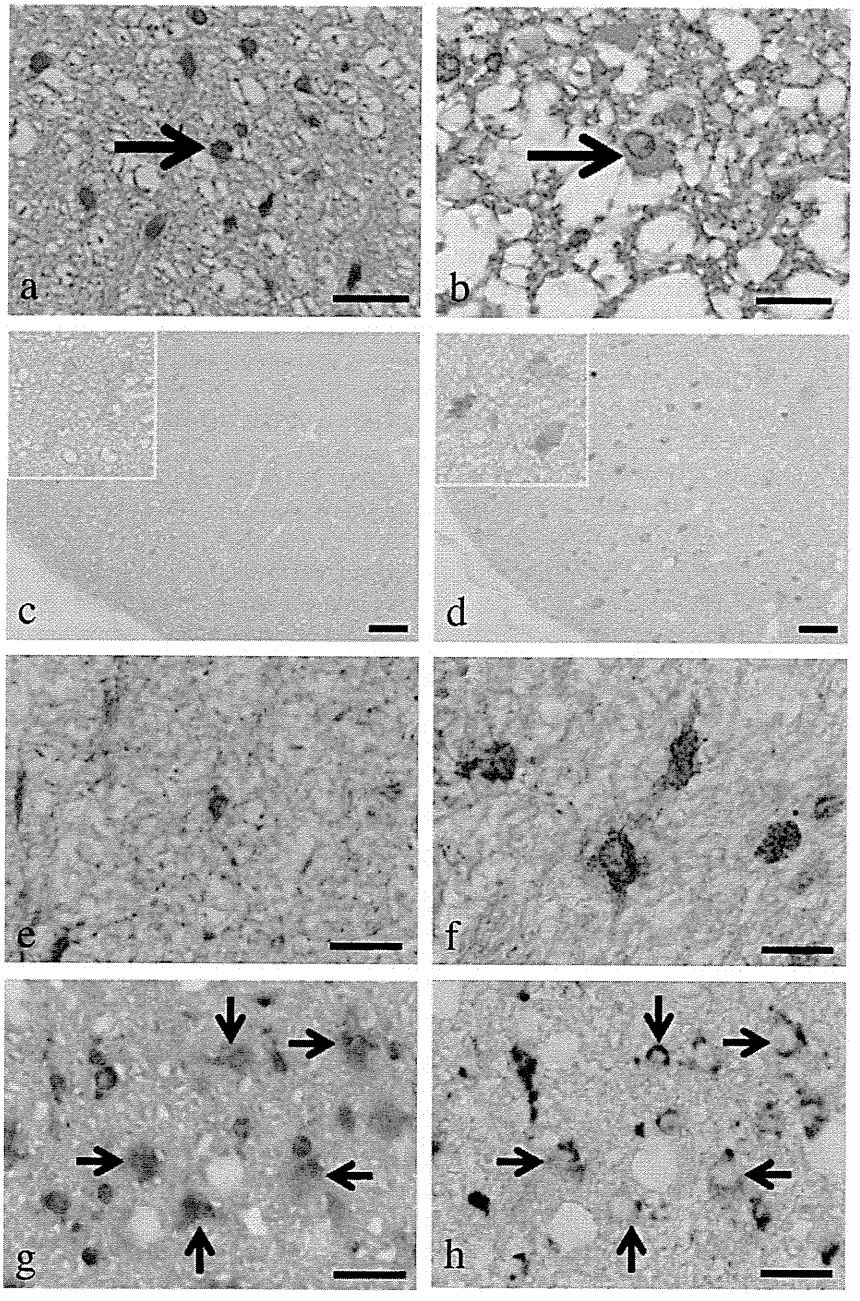

Fig. 5 – Ventral funiculus of the lumbar spinal cord of control (a) and *dmy/dmy* (b) rats aged 8 weeks. Hypertrophic cells with abundant light eosinophilic cytoplasm (arrow) is seen in the *dmy/dmy* rat. Arrow in (a) indicates a possible oligodendrocyte. HE bar, 20 μm. Immunohistochemistry for prohibitin in the lumbar spinal cord of control (c) and *dmy/dmy* (d) rats aged 7 weeks. Insets show higher magnification of the prohibitin-positive cells. Many prohibitin-expressing cells are observed in the *dmy/dmy* rat. Bar, 500 μm. Cytochrome oxidase histochemistry in the ventral funiculus of the lumbar spinal cord of control (e) and *dmy/dmy* (f) rats aged 7 weeks. Intensely stained hypertrophic cells are seen in the *dmy/dmy* rat. Bar, 20 μm. Serially stained sections for prohibitin (g) and PLP in situ hybridization (h). Prohibitin-positive hypertrophic cells are also expressed PLP mRNA. Ventral funiculus of the lumbar spinal cord of 7-week-old *dmy/dmy* rat. Bar, 20 μm.

3. Discussion

Previous electron microscopic and morphometric studies have demonstrated no significant differences in the myelin thickness and fiber size between *dmy* and control rats until the 4th week (Kuwamura et al., 2004). From 5 weeks of age, the myelin thickness in *dmy* rats became significantly less than that of controls, indicating that the progress of myelin destruction during maturation of myelinogenesis and that the *dmy* mutation affect the adequate maintenance of myelin (Kuwamura et al., 2004). The present study reveals that the cell densities and total cell numbers of PLP-positive oligodendrocytes are similar in both *dmy* and control rats until the 6th week but that the number rapidly decreases in the *dmy* rat from 7 weeks of age. In the attractin-deficient *mv* rat, a hypomyelination model, the composition and distribution of major myelin proteins are affected in the spinal cord during postnatal development, whereas the number of oligodendrocytes is not affected. These findings suggest an impairment of oligodendrocyte differentiation and/or a failure of oligodendrocyte to produce myelin proteins in *mv* rats (Izawa et al 2008). Jimpy mouse with a *Plp* mutation exhibits a dysmyelination in the CNS. Jimpy mice produce little CNS myelin, likely due to a premature death of oligodendrocytes throughout the CNS coincident with active myelination (Knapp et al., 1986; Skoff, 1995). Myelin breakdown in the *dmy* rat is considered to be directly related to the loss of myelin-forming oligodendrocytes.

The increased proliferation activity of OPCs was demonstrated by immunohistochemical examination for bromodeoxyuridine (BrdU) and NG2 in the spinal cord of the shiverer mutant (*shi*), which does not form compact myelin due to a deletion in the myelin basic protein gene (Bu et al., 2004). These data suggest that new oligodendrocytes continue to be generated in the dysmyelinated *shi* spinal cord. In a toxin-induced rodent model of demyelination, OPCs increase their expression of Nkx2.2 and Olig2, suggesting that an increased expression of two transcription factors plays an important role in the differentiation of OPCs into remyelinating oligodendrocytes (Fancy et al., 2004). We observed increased NG2+ OPCs in the spinal cord of *dmy* rat compared with the control between the 6th and 7th weeks. This period is consistent with the stage of myelin breakdown in *dmy* rats. Therefore, increased OPCs may try to differentiate into oligodendrocytes and to compensate for the degenerating oligodendrocytes. Nevertheless, myelin collapse develops and the number of OPCs is rapidly decreased at the 8th week.

Positional cloning revealed that the *dmy* rat has a point mutation generating a novel splicing acceptor site in intron 3 of the Mrs2 gene (Kuramoto et al., 2011). Mrs2 encodes an essential component of the major electrophoretic Mg^{2+} influx system in mitochondria of yeast as well as human cells. Our previous electron microscopic study demonstrated the increased number of mitochondria in the cytoplasm of oligodendrocytes in the *dmy* rat. In human mitochondrial disease, increased numbers and abnormal morphology of mitochondria is often observed in the neurons and skeletal muscle, both of which are considered to be a compensatory response to the respiratory dysfunction.

Furthermore, the *dmy* rat has elevated serum lactic acid levels with the progression of the ataxia (Kuramoto et al., 2011). In the present study, we found many oligodendrocytes with abundant cytoplasm that were intensely stained with prohibitin and cytochrome oxidase. This finding reflects the increased number of mitochondria in the oligodendrocytes during the stage of myelin destruction. This increase may be due to the compensation for dysfunction of energy production and suggests that the myelin breakdown in the *dmy* rat is related to the dysfunction of mitochondria in myelin-forming cells. An abnormal iron accumulation and significant upregulation of the antioxidant enzyme heme oxygenase-1 and iron storage protein ferritin has been proved in the *dmy* rat. These findings indicate that iron-mediated oxidative stress is most likely involved in the myelin breakdown of the *dmy* rat and that oligodendrocytes may be primarily affected by the oxidative stress (Izawa et al., 2010). Mice with *Plp1* duplications (*Plp1* tg) have major mitochondrial deficits with a 50% reduction in ATP, a drastically reduced mitochondrial membrane potential and increased numbers of mitochondria (Hüttemann et al., 2009). This finding may imply intriguing relation between the myelin formation and energy metabolism in oligodendrocytes.

Mrs2 gene expression in the CNS was more dominantly observed in neurons than oligodendrocytes (Kuramoto et al., 2011). On the other hand, enhanced expression of prohibitin immunohistochemistry was found in the oligodendrocytes, not in the neurons. There is no apparent abnormality in the neurons of *dmy* rats. Myelination requires a complicated interaction between the axons and processes of oligodendrocytes. Thus, the precise pathogenesis of myelin destruction in the *dmy* rat remains to be elucidated.

In conclusion, the *dmy* rat suffers from mitochondrial dysfunction, which results in increased numbers of mitochondria and hypertrophy of oligodendrocytes, leading to myelin destruction. The *dmy* rat may serve as an excellent animal model for studying the relationship between the energy metabolism in oligodendrocytes and the maintenance and/or production of myelin.

4. Experimental procedure

4.1. Animals

The original *dmy* rat was discovered in a stock of Sprague–Dawley (SD) rats. The congenic *dmy* rat with a WTC background was established and maintained at Kyoto University in Japan. The WTC.DMY-*dmy* (NBRP#0021) strain was supplied by the National BioResource Project-Rat, Kyoto University (Kyoto, Japan), and used for this study. We mated heterozygous females (*dmy*/+) with heterozygous males (*dmy*/+) and obtained both homozygous and control rats (*dmy*/+ or +/+). The genotypes were evaluated by PCR and restriction enzyme fragmentation pattern of the causative gene, Mrs2 (Kuramoto et al., 2011). Animals were handled according to the Guidelines for Animal Experimentation, Osaka Prefecture University.

4.2. *Immunohistochemistry*

Rats were deeply anesthetized and perfused transcardially with 4% paraformaldehyde (PFA) in 0.1 M phosphate buffer (PB; pH 7.4) at 4, 6, 7, and 8 weeks of age. Tissue samples from thoracic and lumbar spinal cords were routinely processed and embedded in paraffin. Five-micrometer sections were dewaxed, pretreated in a microwave with citrate buffer (pH 5.0, 10 mM) for 10 min, and incubated in 3% hydrogen peroxide for 10 min. Sections were then incubated overnight at 4 °C with anti-prohibitin mouse monoclonal antibody for mitochondrion (1:1000; AnaSpec) (Coates et al., 2001). After washes in phosphate-buffered saline (PBS), sections were treated with a peroxidase-conjugated anti-mouse IgG antibody (Histofine Simple Stain MAX PO; Nichirei, Japan) for 45 min. Signals were visualized with a 3,3-diaminobenzidine (DAB) substrate kit (Vector Laboratories, USA). Sections were lightly counterstained with hematoxylin.

For the detection of oligodendrocyte precursor cells (OPCs), NG2 and OLIG2 immunohistochemistry was applied for frozen sections. After washing with PBS, the sections were incubated with anti-NG2 rabbit polyclonal (1:1000; Chemicon) or anti-OLIG2 rabbit polyclonal (1:1000; Immuno-Biological Laboratories) antibodies. Horseradish peroxidase-conjugated polymer (Histofine Simple Stain MAX PO; Nichirei, Tokyo, Japan) was used as a secondary antibody. Signals were visualized with a 3,3-diaminobenzidine substrate kit (Vector Laboratories).

4.3. *Cytochrome oxidase histochemistry*

Frozen spinal cord sections were prepared. Then, 100 μl of freshly prepared reaction buffer [50 mM Tris/HCl (pH 7.4), 0.5 mg/ml diaminobenzidine, 20 μg/ml catalase, and 0.5 mg/ml cytochrome c] was added to each section and slides were incubated for 30 min at 37 °C.

4.4. *In situ hybridization for PLP mRNA*

For riboprobe preparation, a 568 bp fragment of the rat *PLP* cDNA (GenBank accession no. NM_0309906539) was amplified by PCR (forward primer, 5′-TTT GGA GTG GCA CTG TTC TG-3′, nucleotide position 201–220; reverse primer, 5′-GAA AAG CAT TCC ATG GGA GA-3′, nucleotide position 749–768). The PCR product was subcloned into pGEM T-Easy Vector (Promega, USA). Digoxigenin (DIG)-labeled sense or antisense riboprobe was synthesized with SP6 or T7 RNA polymerase (Roche, Switzerland), respectively. For in situ hybridization, lumbar spinal cords were fixed in 4% PFA in 0.1 M PB at 4 °C overnight, treated with 30% sucrose in PBS at 4 °C for 2 or 3 days, and frozen at −80 °C. Ten-micrometer transverse sections were cut on a cryostat. The in situ hybridization procedure was carried out as reported (Sim et al., 2002). Before hybridization, sections were pretreated as follows: 1) 4% PFA in PBS for 15 min, 2) 10 μg/ml proteinase K (Invitrogen, USA) at 37 °C for 12 min, 3) 0.2 M HCl for 10 min, 4) 0.25% acetic anhydride in 0.2 M triethanolamine (pH 8.0) for 10 min. DIG-labeled riboprobes were diluted in hybridization buffer (50% formamide, 10 mM Tris–HCl, pH 8.0, 200 μg/ml yeast tRNA, 10% dextran sulfate, 1× Denhardt's solution, 600 mM NaCl, 0.25% SDS, 1 mM EDTA) and were placed on each slide. Sections were then coverslipped and incubated at 65 °C for 16 h. After hybridization, sections were rinsed in 2× sodium saline citrate (SSC) containing 50% formamide at 65 °C for 30 min, treated with 20 μg/ml RNase A (Roche) at 37 °C for 30 min, and rinsed in 2×, 0.2×, and 0.1× SSC (each at 65 °C for 20 min). RNA hybrids were immunostained with alkaline phosphatase-conjugated anti-DIG antibody (1:1000; Roche) at 4 °C overnight and were visualized with BCIP/NBT substrate (Roche).

4.5. *Image analysis*

Tissue sections were captured with a light microscope (BX41; Olympus, Japan) and a digital camera (DS-Fi1; Nikon, Japan). Transverse spinal cord sections for NG2 immunohistochemistry and PLP in situ hybridization were collected from three different animals in each experimental group. The positive cells were counted in the dorsal and lateral funiculus using image-analyzing software (WinRoof; Mitani Corporation, Japan).

4.6. *Cell counts*

Three different transverse sections from three different animals were evaluated at 6 and 7 weeks of age. The data are presented as the number of NG2- and PLP-positive cells per square millimeters.

4.7. *Statistical analysis*

Data are presented as the means ± standard deviation. Statistical analysis was performed using one-way analysis of variance followed by Tukey's test. A value of P less than 0.05 was considered statistically significant.

Acknowledgments

We are thankful to the National BioResource Project-Rat (http:///www.anim.med.kyoto-u.ac.jp/NBR/) in Japan for providing WTC.DMY-*dmy* (NBRP#0021) rat strain. This work was supported by Grant-in-Aid for Scientific Research from Japan Society for Promotion of Science (JSPS; no. 20580341).

Appendix A. Supplementary data

Supplementary data to this article can be found online at doi:10.1016/j.brainres.2011.03.009.

REFERENCES

Al-Saktawi, K., McLaughlin, M., Klugmann, M., Barrie, S.J., McCulloch, M.C., Montague, P., Kirkham, D., Nave, K.A., Griffiths, I.R., 2003. Genetic background determines phenotypic severity of the Plp rumpshaker mutation. J. Neurosci. Res. 72, 12–24.

Bu, J., Banki, A., Wu, Q., Nishiyama, A., 2004. Increased NG2+ glial cell proliferation and oligodendrocyte generation in the hypomyelinating mutant shiverer. Glia 48, 51–63.

Coates, P.J., Nenutil, R., McGregor, A., Picksley, S.M., Crouch, D.H., Hall, P.A., Wright, E.G., 2001. Mammalian prohibitin proteins respond to mitochondrial stress and decrease during cellular senescence. Exp. Cell Res. 265, 262–273.

Duncan, I.D., Lunn, K.F., Holmgren, B., Urba-Holmgren, R., Brignolo-Holmes, L., 1992. The taiep rat: a myelin mutant with an associated oligodendrocyte microtubular defect. J. Neurocytol. 21, 870–884.

Fancy, S.P., Zhao, C., Franklin, R.J.M., 2004. Increased expression of Nkx2.2 and Olig2 identifies reactive oligodendrocyte progenitor cells responding to demyelination in the adult CNS. Mol. Cell. Neurosci. 27, 247–254.

Griffiths, I.R., 1996. Myelin mutants: model systems for the study of normal and abnormal myelination. BioEssays 18, 789–797.

Hüttemann, M., Zhang, Z., Wullins, C., Bessert, D., Lee, I., Nave, K.A., Appikatla, S., Skoff, R.P., 2009. Different proteolipid protein mutants exhibit unique metabolic defects. ASN Neuro. 1, 165–180.

Izawa, T., Takenaka, S., Ihara, H., Kotani, T., Yamate, J., Franklin, R.J.M., Kuwamura, M., 2008. Cellular responses in the spinal cor during development of hypomyelination in the mv rat. Brain Res. 1195, 120–129.

Izawa, T., Yamate, J., Franklin, R.J.M., Kuwamura, M., 2010. Abnormal iron accumulation is involved in the pathogenesis of the demyelinating dmy rat but nor in the hypomyelinating mv rat. Brain Res. 1349, 105–114.

Kitada, M., Rowitch, D.H., 2006. Transcription factor co-expression patterns indicate heterogeneity of oligodendroglial subpopulations in adult spinal cord. Glia 54, 35–46.

Knapp, P.E., Skoff, R.P., Redstone, D.W., 1986. Oligodendroglial cell death in jimpy mice: an explanation for the myelin deficit. J. Neurosci. 6, 2813-1822.

Knapp, P.E., Adjan, V.V., Hauser, K.F., 2009. Cell-specific loss of k-opioid receptors in oligodendrocytes of the dysmyelinating jimpy mouse. Neurosci. Lett. 451, 114–118.

Kuramoto, T., Sotelo, C., Yokoi, N., Serikawa, T., Gonalons Sintes, E., Canto Martorell, J., Guenet, J.L., 1996. A rat mutation producing demyelination (dmy) maps to chromosome 17. Mamm Geneome 7, 890–894.

Kuramoto, T., Kuwamura, M., Tokuda, S., Izawa, T., Nakane, Y., Kitada, K., Akao, M., Guenet, J.L., Serikawa, T., 2011. A mutation in the gene encoding ion channel mediating influx of Mg^{2+} into mitochondria results in demyelination in the rat. PLoS Genet. 7, e1001262.

Kuwamura, M., Kanehara, T., Tokuda, S., Kumagai, D., Yamate, J., Kotani, T., Nakane, Y., Kuramoto, T., Serikawa, T., 2004. Immunohistochemical and morphometrical studies on myelin breakdown in the demyelination (dmy) mutant rat. Brain Res. 1022, 110–116.

Kwiecien, J.M., O'Connor, L.T., Goetz, B.D., Delaney, K.H., Fletch, A.L., Duncan, I.D., 1998. Morphological and morphometric studies of the dysmyelinating mutant, the Long Evans shaker rat. J. Neurocytol. 27, 581–591.

Sim, F.J., Zhao, C., Penderis, J., Franklin, R.J.M., 2002. The age-related decrease in CNS remyelination efficiency is attributable to an impairment of both oligodendrocyte progenitor recruitment and differentiation. J. Neurosci. 22, 2451–2459.

Skoff, R.P., 1995. Programmed cell death in the dysmyelinating mutants. Brain Pathol. 5, 283–288.

Song, J., Ocnnor, L.T., Yu, W., Baas, P.W., Duncan, I.D., 1999. Microtubule alterations in cultured taiep rat oligodendrocytes lead to deficits in myelin membrane formation. J. Neurocytol. 28, 671–683.

厚生労働科学研究費補助金（創薬基盤推進研究事業）
新規遺伝子変異ラット作製技術に基づく生活習慣病・難治性疾患モデルラットの開発
平成２３年度　研究報告書

発行者　厚生労働科学研究費補助金（創薬基盤推進研究事業）
新規遺伝子変異ラット作製技術に基づく生活習慣病・難治性疾患モデルラットの開発
研究代表者　　中尾　一和

連絡先：〒606-8507　京都市左京区聖護院川原町
京都大学大学院医学研究科　内分泌代謝内科
TEL：075-751-3168